Roughening of porous SiCOH materials in fluorocarbon plasmas

F. Bailly, T. David, T. Chevolleau, Maxime Darnon, N. Posseme, R. Bouyssou, J. Ducote, O. Joubert, Christophe Cardinaud

Roughening of porous SiCOH materials in fluorocarbon plasmas

F. Bailly,[1] T. David,[2,3] T. Chevolleau,[3] M. Darnon,[3,a)] N. Posseme,[2] R. Bouyssou,[3] J. Ducote,[1,2,3] O. Joubert,[3] and C. Cardinaud[4]
[1]*STMicroelectronics, Central R&D, 850 rue J. Monnet, 38926 Crolles Cedex, France*
[2]*CEA-LETI-MINATEC, 17 rue des martyrs, 38054 Grenoble Cedex 09, France*
[3]*LTM/CNRS, CEA-LETI-MINATEC, 17 rue des martyrs, 38054 Grenoble Cedex 09, France*
[4]*Institut des Matériaux Jean Rouxel, CNRS, Université de Nantes, BP 32229, 44322 Nantes Cedex 3, France*

(Received 30 March 2010; accepted 8 May 2010; published online 9 July 2010)

Porous SiCOH materials integration for integrated circuits faces serious challenges such as roughening during the etch process. In this study, atomic force microscopy is used to investigate the kinetics of SiCOH materials roughening when they are etched in fluorocarbon plasmas. We show that the root mean square roughness and the correlation length linearly increase with the etched depth, after an initiation period. We propose that: (1) during the first few seconds of the etch process, the surface of porous SiCOH materials gets denser. (2) Cracks are formed, leading to the formation of deep and narrow pits. (3) Plasma radicals diffuse through those pits and the pore network and modify the porous material at the bottom of the pits. (4) The difference in material density and composition between the surface and the bottom of the pits leads to a difference in etch rate and an amplification of the roughness. In addition to this intrinsic roughening mechanism, the presence of a metallic mask (titanium nitride) can lead to an extrinsic roughening mechanism, such as micromasking caused by metallic particles originating form the titanium nitride mask.
 [doi:10.1063/1.3446820]

I. INTRODUCTION

The most serious challenges in semiconductor manufacturing are to produce low cost integrated circuits with increasing integration densities and to develop high performance devices. An important problem that we are facing today is that electrical signal propagation through metal interconnects is delayed by the resistance (R) in the metal lines and the capacitance (C) between adjacent metal lines. One of the ways to decrease the RC product and thus the runtime delay is to use low dielectric constant materials such as porous SiCOH. However, the use of porous SiCOH implicates several serious issues since one of the main integration difficulties of such materials is their sensitivity to plasma processes leading to material modifications[1–4] and roughening.[5–8] After the patterning of dual damascene structures, the modification and roughening of the sidewalls and bottom of the trenches induce severe electrical and reliability issues.[9]

In particular, the roughness on the sidewalls or bottom in the range of a few nanometers can lead to

(1) non conformal barrier deposition which can induce copper diffusion,[10]
(2) a change in barrier and copper microstructure which can increase the copper resistivity,[11,12]
(3) a variability of critical dimension along the lines which can induce both a change in interline capacity and copper line resistivity.[13–15]

In this work, we investigate the roughening of porous SiCOH when exposed to fluorocarbon based plasmas using atomic force microscopy (AFM) measurements. This study is mainly devoted to the understanding of the roughening mechanism on blanket wafers which is similar to the roughness at the bottom of the trenches. The effect of a metallic mask on the roughening of porous SiCOH is also addressed.

II. EXPERIMENTAL SETUP

A. Materials

The investigated coupons (25 cm^2) are prepared from 300 mm diameter silicon wafers coated with three different dielectric low-k materials deposited by plasma enhanced chemical vapor deposition (PECVD): (1) a porous SiCOH with 28% of porosity, (2) a porous SiCOH with 25% of porosity, and (3) a dense SiCOH with 8% intrinsic porosity. SiCOH materials are also called SiOCH in the literature. More details about the low-k materials are given in Table I.

B. Etching chambers

The etching experiments are mainly performed in an eMax™ etching chamber dedicated for oxide etching. The eMax™ etcher from Applied Materials generates capaci-

TABLE I. Characteristics of the dielectric materials.

Material	Deposition method	Porosity (%)	Density (g cm^{-3})	Dielectric constant
Porous SiCOH (28%)	PECVD	28	1	2.35
Porous SiCOH (25%)	PECVD	25	1.1	2.5
Dense SiCOH	PECVD	8	1.3	2.9

a)Electronic mail: maxime.darnon@cea.fr.

tively coupled plasmas. A 200 mm diameter carrier wafer sits on the powered electrode supplied by a rf generator operated at 13.56 MHz. This MERIE (magnetically enhanced reactive ion etching) reactor is surrounded by four electromagnets which produce a rotating magnetic field (0.5 Hz and 0 to 200 Gauss) leading to an increase in plasma density. For all etch processes, the magnetic field is kept constant at 20 G. The wafers are clamped using an electrostatic chuck and the temperature of the wafer is kept at 15 °C by means of a helium backside temperature regulation at 14 Torr. Studies in this chamber are performed using coupons of the wafers of interest, patched on 200 mm carrier silicon wafers coated with thermal oxide. The 25 cm^2 coupon is thermally connected to the temperature regulation using Fomblin™ vacuum grease between the carrier wafer and the coupon.

Some additional experiments are also performed in a Kiyo™ chamber from LAM Research Corporation. This chamber generates high density transformer coupled plasmas (TCP) using a source frequency of 13.56 MHz. The 300 mm diameter wafer sits on an electrode powered independently at 13.56 MHz to control the ion energy. Studies in this chamber are performed on the full wafers of interest.

C. AFM measurements

AFM measurements are performed at ambient atmosphere with a Nanoscope III multimode microscope from Digital Instruments. To minimize the interaction between the tip and the sample, tapping mode was preferred to the contact mode. In the tapping mode AFM,[16] a cantilever oscillates with the probing tip close to its free resonance frequency (with a given amplitude). The interaction between the sample and the probe gives rise to a shift in the probe vibration amplitude measured in a free oscillation, i.e., with the probe far away from the sample. The vertical displacement (height) needed to keep the set amplitude provides information about the topography of the sample. Data are acquired for a scanned area of 1×1 μm^2 having 512×512 data points. The silicon tips have a curvature radius of about 10 nm which provides a lateral resolution in the range of 10 nm. The tapping frequency is 5% lower than the resonance one (about 235 kHz) and the free-air amplitude is chosen between 10 and 13 nm. The ratio between the amplitude setpoint A_{sp} and the free amplitude A_0 is taken in soft-tapping conditions ($A_{sp}/A_0=0.85$) to prevent damaging the silicon tips.

After removing the slope and curvature of the image, two parameters are measured to describe the roughness: the root mean square (RMS) roughness σ and the correlation length ξ. The RMS roughness describes the vertical extent of the roughness and is given by the standard deviation of the height distribution Z as follows:

$$\sigma = \langle [Z(r) - \mu]^2 \rangle^{1/2},$$

where $r=(x,y)$ is the coordinate of a point on the surface and Z is the height. μ is the mean value of the height, z, across all in-plane coordinates (x,y).

In order to be accurate in the roughness estimation, measurements are performed at five different locations using four reference samples with different surface roughness ranging from 1 to 10 nm. The standard deviation α was measured for each sample and was found to be similar ($\alpha=0.2$ nm) for all samples, except for the sample with the lowest surface roughness ($\alpha<0.1$ nm), as shown in Fig. 1. Based on these results, we can assume that the resolution of our surface roughness measurement is about 0.2 nm. Since the roughness measurement is also linked to the tip-surface convolution, we checked that no major variation in the tip occurred after each image. This was achieved by means of a reference sample which has a surface roughness of about 5 nm. This reference sample is also used to check the tip shape and to change the tip as soon as it gets eroded.

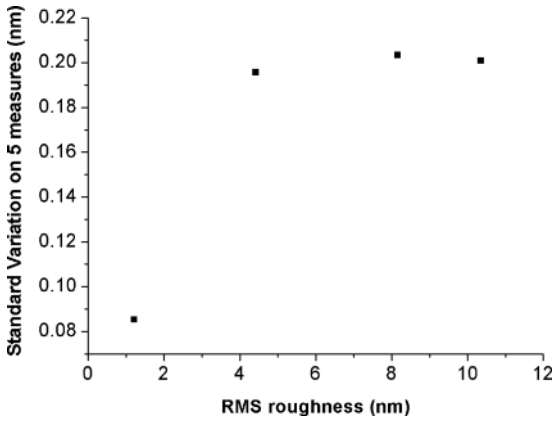

FIG. 1. Standard deviation as a function of the RMS roughness measured with four different samples.

The correlation length ξ represents the lateral extent of the roughness. In most cases, some processes such as deposit growth, ion sputtering, or plasma etching are expected to create a self-affine fractal surface. ξ is defined as the upper limit of the observation scale where the surface exhibits a self-affine property. Over this scale, the surface can be considered as flat. One can extract the ξ value from the averaged power spectral density (PSD) given by:

$$\mathrm{PSD}(k) = \frac{1}{\mathrm{area}} \left\langle \left| \int\int e^{-ikr} Z(r) \frac{d^2 r}{2\pi} \right|^2 \right\rangle_{|k|=k}, \quad r=(x,y),$$

where k is the spatial frequency. Specifically, the PSD gives the spatial frequency distribution of the surface roughness as shown in Fig. 2. The correlation length is defined by the length of the PSD saturation frequency which is obtained by fitting the experimental log-log PSD graph. In this work, the correlation length is simply determined by taking the intersection between the PSD saturation line and high frequency line from the PSD graph. The accuracy is estimated to be 20%.

D. Surface analyses techniques

The surface composition of porous SiCOH materials after plasma exposure is investigated by means of x-ray photoelectron spectroscopy (XPS). XPS analyses are carried out on coupons of 300 mm diameter wafers patched on 200 mm carrier wafers. The spectra are collected with a Fisons surface systems ESCALAB 220i operating with an Al K_α x-ray

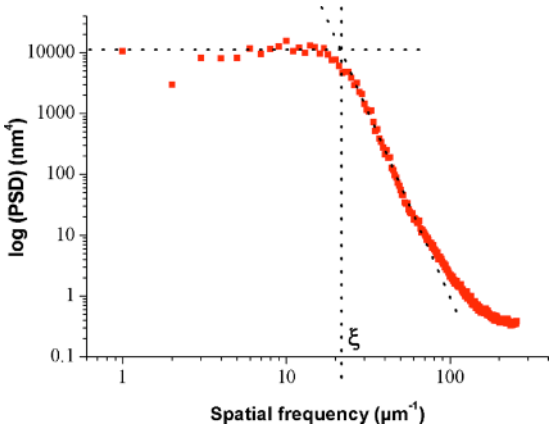

FIG. 2. (Color online) Determination of the correlation length by taking from the log-log PSD graph the intersection between the PSD saturation line and the high frequency line.

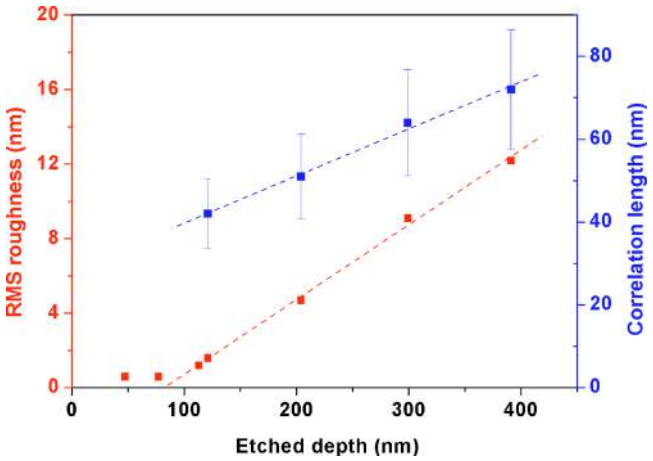

FIG. 3. (Color online) RMS roughness (a) and correlation length (b) as a function of the etched depth of porous SiCOH (25%) using a CF_4/Ar plasma.

source ($h\nu$=1486.6 eV) and an electron energy analyzer operating in a constant pass energy mode of 20 eV. Chemical compositions are derived from the respective areas of the different XPS spectra. Spectral decomposition is performed to extract the Si 2*p*, O 1*s*, C 1*s*, N 1*s*, and F 1*s* peak intensities. Individual line shapes are simulated with the combination of Lorentzian and Gaussian functions. The background subtraction is performed by using a Shirley function. After XPS analysis, the integrated intensities are divided by the theoretical Scofield cross section[17] (C 1*s*:1; O 1*s*:2.93; Si 2*p*:0.82; F 1*s*:4.43; N 1*s*:1.8). The sum of the concentration of the different elements present on the analyzed surface is equal to 100%. The hydrogen content is not taken into account in this calculation since hydrogen cannot be detected by XPS. More details of the experimental characterization conditions can be found elsewhere.[3,18]

III. EXPERIMENTAL RESULTS

The surface roughening of porous SiCOH is investigated in fluorocarbon based plasmas. The etching experiments are performed in the eMax™ chamber using coupons of SiCOH wafers stuck on a 200 mm diameter silicon dioxide carrier wafer.

Figure 3 shows the RMS roughness and correlation length as a function of the etched depth for a p-SiCOH film (25% of porosity) etched in a CF_4/Ar plasma. The RMS roughness presents an initiation period during the first etched 95 nm, followed by a linear increase with a rate of 4%+/−0.8 (4 nm of RMS roughness is measured when 100 nm of porous SiCOH is etched). The RMS roughness goes from 0.5 to more than 12 nm for an etched depth close to 400 nm. The correlation length also presents a linear increase with the etched depth, indicating a lateral extension of the roughness as visible on the top view SEM pictures of Fig. 4.

The effect of the porosity on the surface roughening in fluorocarbon based plasmas is studied by comparing the behavior of a dense SiCOH and two porous SiCOH with two different porosities (25% and 28%). The Fig. 5 shows that the surface of the dense material remains smooth with a RMS roughness of 0.5 nm when exposed to a CF_4/Ar plasma. On the contrary, porous SiCOH materials show an increase in the RMS roughness with the etch time which is more pronounced for the porous material with the 28% porosity. Increasing the porosity from 25% to 28% leads to an increase in the RMS roughness of around 2 nm for a given etched depth. The porous material with the highest porosity (28%) presents no significant initiation period and a slope close to 3.5%+/−0.7 in the linear regime.

The impact of the etch chemistry on the porous SiCOH roughening is investigated in Fig. 6 by comparing the RMS roughness induced by two different fluorocarbon based etch chemistries (more or less polymerizing). Going to a more polymerizing process (from CF_4/Ar to $CF_4/Ar/CH_2F_2$), a slow down of the roughening is clearly observed with an increase in the initiation period (from 95 to 160 nm), and a decrease in the roughening rate (from 4% to 2%) in the linear regime. The roughness evolution when the material is exposed to a pure argon plasma is also reported in this figure. In this later case, no roughening of the material is observed.

The results show that the surface roughening of SiCOH films in fluorocarbon based plasmas depends on the etched depth, the porosity, and the plasma chemistry. The RMS roughness presents an initiation period followed by a linear increase with the etched depth. The correlation length increases with the etched depth, indicating a lateral extension of the roughness. The RMS roughness is more pronounced on more porous materials, and with less polymerizing process conditions.

IV. DISCUSSION

The evolution of the roughness during plasma etch processes has already been studied.[5,7,8,19–25] Plasma processes are usually known to smooth the etched surface. The isotropic component of the etch process,[19,20] as well as the shadowing effect[26,27] and the preferential sputtering of the material for off-normal ions[8,28,29] contribute to this effect during plasma etch processes.

Nevertheless, several groups have reported that the surfaces could also be roughened when exposed to plasma etch processes.[25,30–33] Several explanations such as preferential etching by re-emitted species[30,31] or ion induced defects[32]

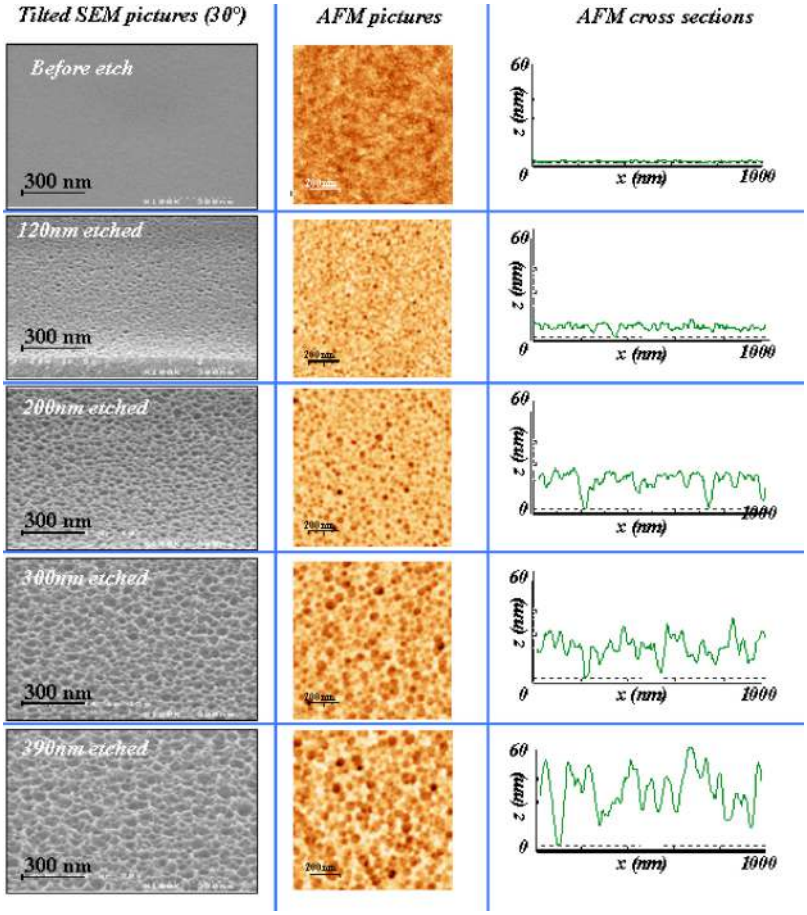

FIG. 4. (Color online) Tilted SEM pictures, AFM top down pictures, and AFM cross sections for different porous SiCOH (25%) etched depths in a CF_4/Ar plasma.

have been proposed. However, recent studies[25,33] tend to prove that etch induced roughness rather comes from a micromasking induced by chamber wall particles sputtered during the etch process.

In the case of SiCOH materials, etch induced roughness has also been observed.[5–8] In those papers, the fluorocarbon species deposited on the porous low-k surface are supposed to be responsible for the material roughening. Tatsumi and Urata[34] propose that low-k materials are roughened when a thin fluorocarbon layer (~4 nm) is deposited on the material surface, while no fluorocarbon or thicker fluorocarbon layers do not lead to roughening. Yin *et al.*[6,7] attribute the etch induced roughness to a micromasking on the surface by the fluorocarbon species deposited on the material surface. They attribute the non uniform coverage of the surface to the presence of pores in the material. Lazzeri *et al.*[5] propose that the larger surface of porous materials leads to an incomplete coverage of the surface of the dielectric by the fluorocarbon layer, compared to dense dielectrics. Due to this incomplete coverage, plasma species can directly interact with the low-k material, leading to harsher etch conditions and roughness. In both cases, the models assume that the roughness is cre-

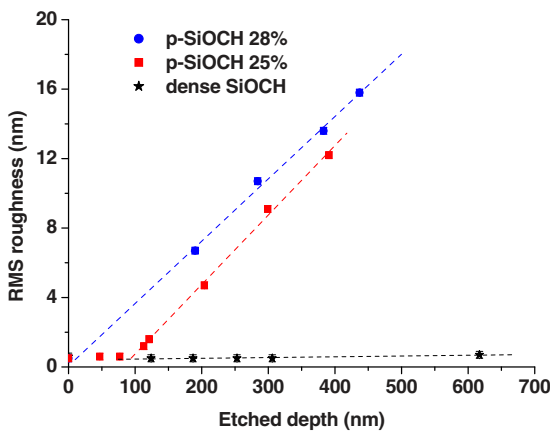

FIG. 5. (Color online) RMS roughness as a function of the etched depth for porous SiCOH (25%), porous SiCOH (28%), and dense SiCOH using a CF_4/Ar plasma.

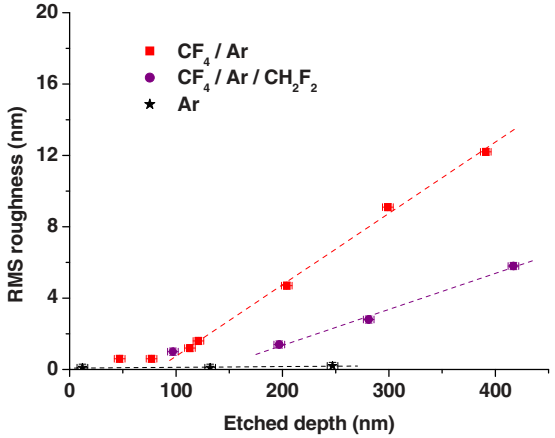

FIG. 6. (Color online) RMS roughness as a function of the etched depth for porous SiCOH (25%) using a CF_4/Ar, a $CF_4/Ar/CH_2F_2$, or a pure Ar plasma.

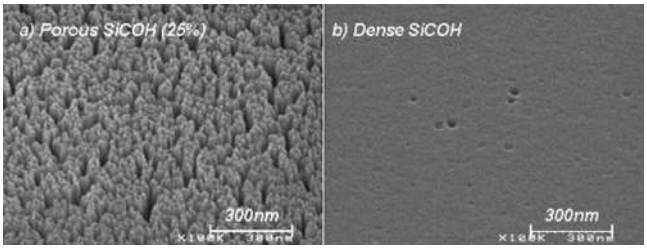

FIG. 7. Tilted (30°) SEM pictures of porous SiCOH (a) and dense SiCOH (b) etched in a SF_6 plasma.

ated by an incomplete or nonhomogeneous coverage of the porous SiCOH surface by fluorocarbon species.

Our experimental results show that the RMS roughness of porous SiCOH increases linearly with the etched depth. On the contrary, the dense SiCOH presents no roughening with the same process conditions. The absence of roughness on the dense material lets us rule out the micromasking from chamber wall particles during the etch process as the cause of the roughening.

In order to investigate the role of the fluorocarbon species on the roughness formation, a dense and a porous SiCOH (25% of porosity) film have been etched in a Kyio™ chamber using a SF_6 plasma. In Fig. 7, we can clearly see that the surface of the porous SiCOH material is very rough (8.1 nm of RMS roughness) after 270 nm of etching, while the dense SiCOH stays smooth. In these conditions, XPS analyzes show that the surface of the porous SiCOH is made of 32% of Si, 48% of O, 4% of C, and 16% of F (*ex situ* analysis). The carbon peak energy is centered around 286 eV, indicating no significant fluorocarbon deposition on the porous SiCOH surface. These additional experiments show that the fluorocarbon layer formed on the porous SiCOH cannot be directly responsible for the porous SiCOH roughening. Thus, the porous SiCOH roughening cannot be attributed to a micromasking by fluorocarbon species, or to any mechanism involving a fluorocarbon layer.

Our experiments, as well as Lazzeri *et al.*,[5] show that the RMS roughness increases linearly with the etched depth. Both data also show an increase in the roughness with the porosity of the material. The linear behavior is remarkable since it shows that the height of the features on the surface of the material keeps increasing with the etched depth. Looking at Fig. 4, we can clearly see that the features look like pits, with a diameter which is increasing with the etched depth. The depth of the pits increases also with the material etched depth. It is clear that different sizes of pits are present, indicating the continuous formation of pits during the etch process (larger pits are supposed to be formed earlier). The pits are very narrow and deep. Due to the limitation of the AFM (diameter and height of the tip), it is assumed that the pits extend even deeper and narrower than seeable in Fig. 4. This means that during the etch process, pits with important aspect ratio (more than 10) and very small diameter (few nanometers) are formed. The linear increase in the pit depth with the etched depth shows that the bottom of the pit is etched faster than the top "flat" surface. In other words, the etch rate of the top "flat" surface is lower than the etch rate at the bottom of the pits.

This observation is pretty non obvious, since it is well known in the field of plasma etching that the etch rate usually decreases when the aspect ratio of the features to be etched increases.[35,36] This so called RIE lag (reactive ion etching lag) or aspect ratio dependant etching effect leads to uniformity issues for contact or via etching. In our conditions, we are etching pits which are comparable to few nanometers wide vias or contacts. No mask is used on those pits. Since the pit depth increases with the top "flat" surface etched depth, the etch rate is larger at the bottom of the pit, i.e., in the features with a high aspect ratio, than on the top "flat" surface, i.e., features with small aspect ratio. This kind of evolution is quite unusual but has already been identified as inverse RIE lag.[37,38] The origin of the inverse RIE lag is explained by the difference in neutral and ion flux reaching the bottom of vias for different aspect ratios.[37,38] Usually, inverse RIE lag is observed in a quite narrow process window. In our conditions the roughness increases on a wide range of process conditions, as soon as the material is porous. Furthermore, the aspect ratio of the top flat surface is equal to zero, while the aspect ratio of the pits is larger than ten. No inverse RIE lag has ever been reported with such a large range of aspect ratios, as far as we know. Thus, the origin of the linear increase in the RMS roughness cannot be directly attributed to geometrical factors and differences in neutral and ions flux between the features.

Since the roughening only occurs on the porous material, the origin of the larger etch rate at the bottom of the pits than on the "flat" top surface must be attributed to specificities of porous materials.

(1) It is known that the surface of porous materials gets denser on few nanometers when it is exposed to plasma processes.[39,40] This densification is mostly attributed to the ion bombardment on the top surface.
(2) Plasma radicals can diffuse and deeply modify the porous SiCOH materials.[3] The etching plasma induced material damage is mostly a loss of carbon and fluorine incorporation. Using attenuated total reflection infrared spectroscopy,[41] we have verified that Si–F bonds are created in the porous SiCOH in our experiments (not presented here).
(3) Porous materials present a larger surface than dense materials. As a consequence, they are more easily chemically etched than the dense SiCOH. As an example, porous SiCOH is etched by a SF_6 plasma even without bias power.[3]

To explain the linear increase in the RMS roughness with the etched depth, we are proposing the following mechanism: the surface of the porous SiCOH gets denser under ion bombardment. At the same time only few ions reach the bottom of the pits because of electrostatic effects.[42] Thus, the material remains porous at the bottom of the pits while the top surface becomes dense. The plasma radicals, in particular free fluorine, diffuse through the pits and the pore network, and modify the porous material at the bottom of the pits, leading to fluorine rich porous silicate. This modified porous material can be etched much faster than the denser material on the top flat surface. Thus, the faster etch rate at

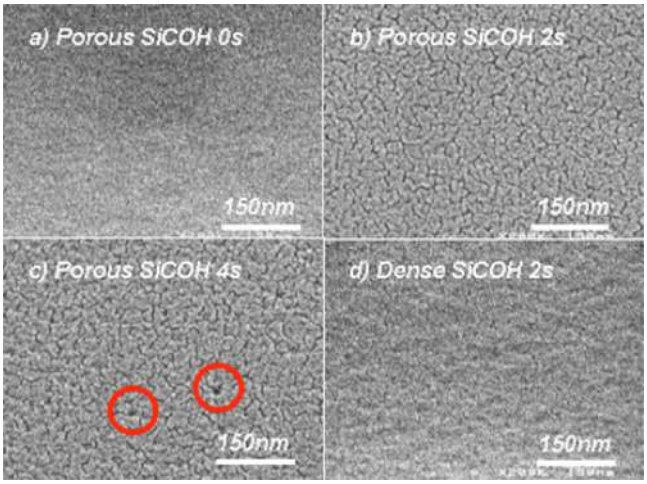

FIG. 8. (Color online) Surface morphology after CF_4/Ar plasma exposure: (a) 0*s* on porous SiCOH (25%), (b) 2*s* on porous SiCOH (25%), (c) 4*s* on porous SiCOH (25%), and (d) 2*s* on dense SiCOH.

the bottom of the pits compared to the top "flat" surface is explained by a difference in material density and composition and by a high chemical etch rate at the bottom of the pits.

For this model to be valid, pits must be present on the surface of the material to be etched. However, looking at the material surface before etching, a very low RMS roughness (0.5 nm) is present, which means that the features on the surface have a small aspect ratio and are not as deep as the denser top surface created during the etch process. In Fig. 8, the surface of the porous SiCOH (25% of porosity) has been observed after 2 and 4 s of plasma processes. In these pictures, we can see the occurrence of cracks on the material surface. Indeed, the denser surface created by the plasma is assumed to present a stress, which results in cracking.[43] Those cracks could then play the role of diffusion paths for the reactive species of the plasma to reach the not as dense material underneath. After 4 s of plasma process, we can see that pits start to be visible where the cracks are merging. This analysis of the first few seconds of the process highlights the formation of features on the porous material surface, which could result in roughening using our model. This observation is consistent with the initiation period observed earlier. Indeed, it takes few seconds (and so few tens nanometers with the etch rate considered here) to create the pits, and then to start roughening the surface of the porous material.

In order to validate our model, a porous SiCOH (25% of porosity) wafer has been exposed to an argon plasma. In those conditions, a similar densification and cracking of the top surface is observed as presented in Fig. 9. However, no pit is formed and the material stays smooth even after 250 nm is etched. Using an argon plasma, no huge chemical modification or etching of the porous material is expected at the bottom of the features, due to the purely physical mechanism of the argon sputtering process. This confirms that the roughening of the surface requires a chemical component for the etch process, that could result in a faster etch rate at the bottom of pits.

Besides, we etched a stack composed of 330 nm thick

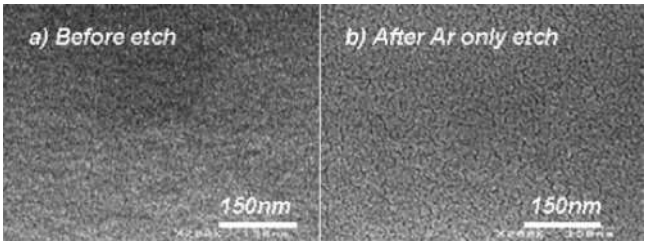

FIG. 9. Surface morphology before (a) and after (b) Ar plasma exposure of porous SiCOH (25%).

porous SiCOH (25% of porosity) coated on the dense SiCOH. As expected and seen in Fig. 10, the RMS roughness and the correlation length increase while the porous SiCOH is etched. When the interface between the porous and the dense SiCOH is reached, a decrease in the RMS roughness is observed, from 8.3 to 6.3 nm. This decrease is directly related to the difference in etch rate between the two materials (1220 nm/min for the porous SiCOH with 25% of porosity and 840 nm/min for the dense SiCOH), which leads to a transfer of the roughness in the same proportions. No variation in the correlation length is observed at the interface. During the dense SiCOH etching, the RMS roughness hardly evolves, while the correlation length linearly increases with a larger slope than observed on porous SiCOH. Due to the variation on the data points, we cannot tell if the RMS roughness decreases or stays constant during the dense SiCOH etching. However, it is clear that the variation is low, and that the RMS roughness does not increase, which means that the roughness created is not transferred during the dense SiCOH etching. The increase in the correlation length indicates that the surface tends to be smoothed by the process, as usually seen in etch processes. This experiment lets us conclude that the porosity is not only necessary to initiate the roughness, but also leads to its amplification during the dielectric etch process. If the material is dense, no significant densification occurs on its surface, and no significant diffusion of species takes place to modify the material and amplify the chemical etch component. Thus, no difference in etch rate between the "flat" surface and the bottom of the pits is expected and the roughness does not increase in this case.

Based on all these observations, our model can be summed up as the following: during the first few seconds of the etch process, the surface of the porous SiCOH gets denser and stressed. The stress in the material results in a cracking of the surface, which creates diffusion paths for the plasma species. At the bottom of the deepest cracks (where the cracks are merging), the pristine material is exposed, forming pits on the surface. The pits and the porous network let the free fluorine from the plasma diffuse and modify the material at the bottom of the pits, leading locally to fluorine rich porous silica. Thus the material exposed to the plasma is a dense SiCOH on the "flat" surface, and a fluorine rich porous silica at the bottom of the pits. This difference in material composition and density leads to a difference in etch rate between the surface and the bottom of the pits. The bottom of the pits is etched faster than the surface, leading to an increase in the pit height (i.e., RMS roughness) with the etched depth.

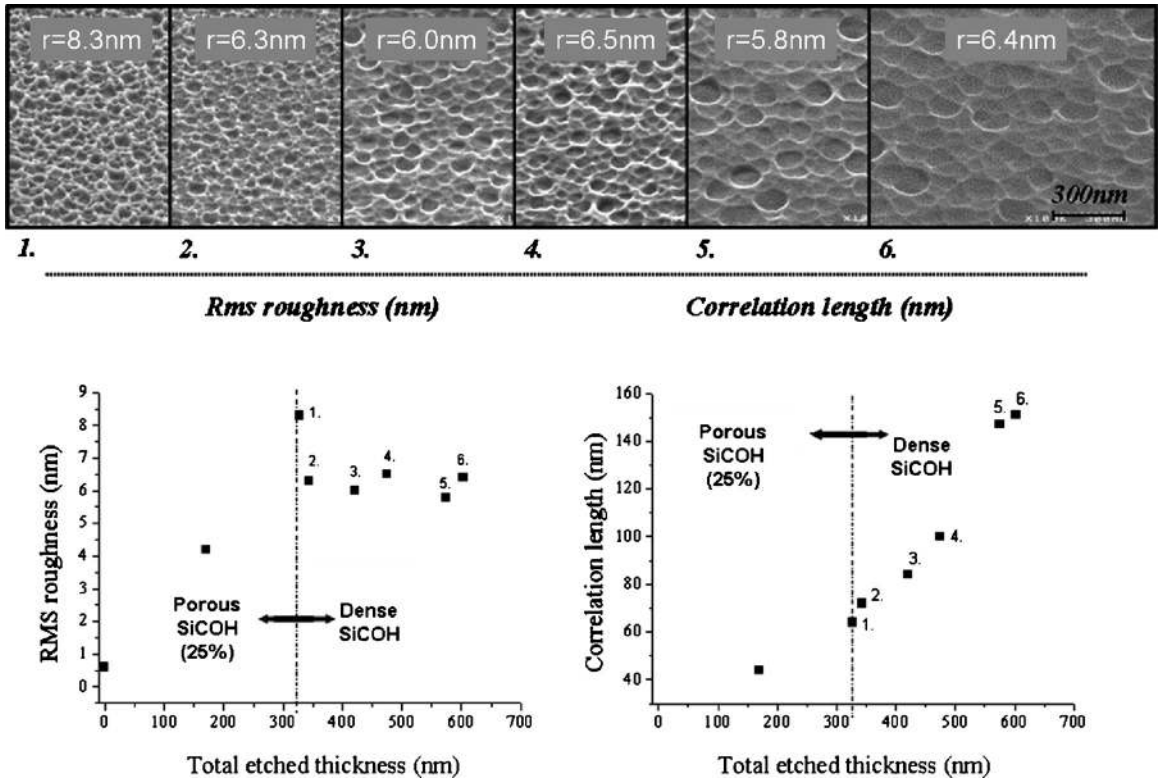

FIG. 10. RMS roughness (a) and correlation length (b) evolution during the etching in CF_4/Ar plasma of a stack made of 330 nm of porous SiCOH (25%) on a dense SiCOH material.

During the etch process, the existing pits are transferred and amplified, while new ones keep forming constantly following the same mechanism. In parallel of the roughening mechanism, the lateral extension of the roughness (due to the isotropic component of the etch process, the shadowing effect and the preferential sputtering of the material for off-normal ions) leads to an increase in the correlation length.

It has to be noticed that this roughening mechanism is expected to remain valid for other kind of porous materials. For example, we have verified the roughening of porous silicon (not presented here), and porous SiO_2 roughening has already been reported by Kwon *et al.*[44]

We have also verified that this mechanism is confirmed in different kind of plasma chambers. Porous SiCOH etched in MERIE, CCP, ICP and TCP industrial reactors present the same roughening behavior (not shown here).

The effect of the plasma polymerizing rate in this model is extremely complex and not fully determined. Indeed, fluorocarbon species dump fluorocarbon polymers on the material surface, which decreases the etch rate. Our experiments have shown that the RMS roughness decreases by increasing the polymerizing rate of the plasma. In our roughening model, going to a more polymerizing plasma can have several effects as follows:

- the deposition of fluorocarbon species can change the surface behavior. Indeed, pits can be sealed by fluorocarbon species as soon as they are created, blocking any further extent of the pit and roughening of the surface. The surface densification and stress can also be different depending on the plasma polymerizing rate. Thus, more or less pits could be formed, leading to a change in the RMS roughness. Indeed, fewer pits are observed when a more polymerizing process is used.
- Fluorocarbon species deposition at the bottom of the pits can prevent material damage,[3] decreasing the etch rate. It is not sure though that much fluorocarbon precursors reach the bottom of the pits, because of the high sticking coefficient of those species and very small diameter of the pits.
- The change in the balance between free fluorine and fluorocarbon species could also change the etch rate both on the "flat" surface and at the bottom of the pits. This could lead to a change in the etch rate ratio between the top and the bottom of the pits, leading to a slower or faster roughening rate.

V. IMPACT OF THE INTEGRATION SCHEME

In the previous part, we have proposed an intrinsic roughening mechanism for porous materials, based on blanket wafer studies. We will now see the impact of the integration scheme on the porous SiCOH roughness.

Several integration schemes involving different masking strategies are in competition nowadays. In particular, several groups use titanium nitride as a hard mask for trenches patterning.[45–47] To investigate the effect of the TiN hard mask on the porous low k roughness, coupons of porous SiCOH (25% of porosity) are patched on a TiN wafer. As seen in Fig. 11, the roughness is much larger with a TiN

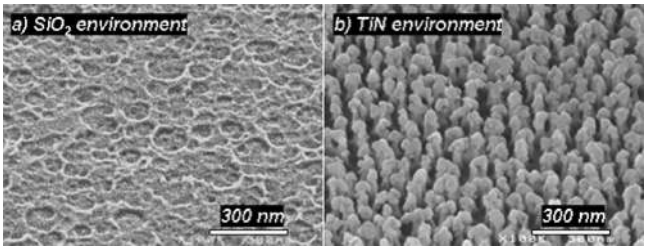

FIG. 11. Tilted SEM picture of porous SiCOH (25%) etched using a CF_4/Ar plasma in a SiO_2 environment (a) or a TiN environment (b).

environment than with a SiO_2 one. Furthermore, the roughness morphology is significantly different. This kind of roughness has already been observed at the bottom of trenches etched in SiCOH using a TiN hard mask.[48,49] XPS analysis of the coupon surface shows 4% of titanium on the surface. This indicates that in addition to the intrinsic roughening of the porous SiCOH in fluorocarbon plasma, an extrinsic roughness can originate from the micromasking of the top surface by metallic particles coming from the TiN etching.[45]

All our results show that porous materials intrinsically get rougher when etched in fluorocarbon based plasmas. When the material gets more porous, this phenomenon is amplified. For the future technological generations, where highly porous dielectrics will be required, the roughening will become a real show stopper. Based on our model, we can propose ways to limit the material roughening as follows:

- polymerizing plasmas are preferred.
- The trenches must be shallow enough, so that the etching is stopped before the end of the initiation period. For example, the $CF_4/Ar/CH_2F_2$ process used on the porous SiCOH (25% of porosity) creates no roughness until 160 nm thick of dielectric is etched. This depth is compatible with metal lines height for the current and future technological nodes.
- Dielectric materials with better mechanical properties (elastic modulus, hardness) are preferred to limit the formation of cracks under plasma exposures.
- The mask should not provide particles susceptible to create a micromasking on the dielectric surface. This can be done by using organic masks or by tuning the etch process conditions when using a metallic mask.[45]

VI. CONCLUSION

In this study, we have investigated the roughening mechanism of SiCOH materials when they are etched in fluorocarbon plasmas. We have shown that the RMS roughness and the correlation length linearly increase with the etched depth. We proposed a roughening mechanism to explain why the bottom of the deep and narrow features is etched faster than the surface. During the first few seconds of the etch process, the surface of porous SiCOH gets denser, and cracks are formed, leading to the formation of deep and narrow pits. Plasma radicals can diffuse into these pits, and through the pore network, to modify the porous material at the bottom of the pits. As a result, there is a difference in material density and composition between the surface and the bottom of the pits, leading to a difference in etch rate, and an amplification of the RMS roughness. In parallel, isotropic etching, shadowing and preferential sputtering by off-normal ions lead to a lateral extension of the roughness. In addition to this intrinsic roughening mechanism, we have shown that the integration scheme can lead to an extrinsic roughening mechanism, such as micromasking from metallic particles originating from TiN hard mask.

ACKNOWLEDGMENTS

The support of Mickael Martin, Denis Mariolle, and Nicolas Chevalier from CEA-LETI-MINATEC is gratefully acknowledged for fruitful discussions and support on the AFM technique.

[1] D. Shamiryan, M. R. Baklanov, S. Vanhaelemeersch, and K. Maex, J. Vac. Sci. Technol. B **20**, 1923 (2002).
[2] D. Eon, V. Raballand, G. Cartry, M.-C. Peignon-Fernandez, and Ch. Cardinaud, Eur. Phys. J.: Appl. Phys. **28**, 331 (2004).
[3] N. Posseme, T. Chevolleau, O. Joubert, L. Vallier, and N. Rochat, J. Vac. Sci. Technol. B **22**, 2772 (2004).
[4] M. Darnon, T. Chevolleau, T. David, N. Posseme, J. Ducote, C. Licitra, L. Vallier, O. Joubert, and J. Torres, J. Vac. Sci. Technol. B **26**, 1964 (2008).
[5] P. Lazzeri, X. Hua, G. S. Oehrlein, M. Barozzi, E. Iacob, and M. Anderle, J. Vac. Sci. Technol. B **23**, 1491 (2005).
[6] Y. Yin, S. Rasgon, and H. H. Sawin, J. Vac. Sci. Technol. A **24**, 2360 (2006).
[7] Y. Yin and H. H. Sawin, J. Vac. Sci. Technol. A **25**, 802 (2007).
[8] Y. Yin and H. H. Sawin, J. Vac. Sci. Technol. A **26**, 151 (2008).
[9] N. Posseme, T. Chevolleau, T. David, M. Darnon, J. P. Barnes, O. Louveau, C. Licitra, D. Jalabert, H. Feldis, M. Fayolle, and O. Joubert, Microelectron. Eng. **85**, 1842 (2008).
[10] J.-N. Sun, Y. Hu, W. E. Frieze, W. Chen, and D. W. Gidley, J. Electrochem. Soc. **150**, F97 (2003).
[11] R. Kumar, T. K. S. Wong, B. R. Murthy, Y. H. Wang, and N. Balasubramanian, J. Electrochem. Soc. **153**, G420 (2006).
[12] G. Brunoldi, K. J. Kozaczek, B. Gittleman, and T. Marangon, Microelectron. Eng. **83**, 2208 (2006).
[13] M. Stucchi, M. Bamal, and K. Maex, Microelectron. Eng. **84**, 2733 (2007).
[14] W. Steinhögl, G. Schindler, G. Steinlesberger, M. Traving, and M. Engelhardt, Microelectron. Eng. **76**, 126 (2004).
[15] L. H. A. Leunissen, W. Zhang, W. Wu, and S. H. Brongersma, J. Vac. Sci. Technol. B **24**, 1859 (2006).
[16] J. Tamayo and R. Garca, Langmuir **12**, 4430 (1996).
[17] J. H. Scofield, J. Electron. Spectrosc. Relat. Phenom. **8**, 129 (1976).
[18] N. Posseme, T. Chevolleau, O. Joubert, L. Vallier, and P. Mangiagalli, J. Vac. Sci. Technol. B **21**, 2432 (2003).
[19] G. M. Gallatin and C. B. Zarowin, J. Appl. Phys. **65**, 5078 (1989).
[20] W. W. Mullins, J. Appl. Phys. **30**, 77 (1959).
[21] R. P. U. Karunasiri, R. Bruinsma, and J. Rudnick, Phys. Rev. Lett. **62**, 788 (1989).
[22] J. H. Yao and H. Guo, Phys. Rev. E **47**, 1007 (1993).
[23] C. Roland and H. Guo, Phys. Rev. Lett. **66**, 2104 (1991).
[24] G. S. Bales and A. Zangwill, Phys. Rev. Lett. **63**, 692 (1989).
[25] M. Martin and G. Cunge, J. Vac. Sci. Technol. B **26**, 1281 (2008).
[26] J. T. Drotar, Y.-P. Zhao, T.-M. Lu, and G.-C. Wang, Phys. Rev. B **61**, 3012 (2000).
[27] E. Zakka, V. Constantoudis, and E. Gogolides, IEEE Trans. Plasma Sci. **35**, 1359 (2007).
[28] M. Schaepkens, G. S. Oehrlein, C. Hedlund, L. B. Jonsson, and H.-O. Blom, J. Vac. Sci. Technol. A **16**, 3281 (1998).
[29] D. Flamm and D. Manos, *Plasma Etching: An Introduction* (Academic, New York, 1989).
[30] Y.-P. Zhao, J. T. Drotar, G.-C. Wang, and T.-M. Lu, Phys. Rev. Lett. **82**, 4882 (1999).
[31] G. S. Hwang, C. M. Anderson, M. J. Gordon, T. A. Moore, T. K. Minton,

and K. P. Giapis, Phys. Rev. Lett. **77**, 3049 (1996).
[32]R. Pétri, P. Brault, O. Vatel, D. Henry, E. André, P. Dumas, and F. Salvan, J. Appl. Phys. **75**, 7498 (1994).
[33]E. Gogolides, C. Boukouras, G. Kokkoris, O. Brani, A. Tserepi, and V. Constantoudis, Microelectron. Eng. **73–74**, 312 (2004).
[34]T. Tatsumi and K. Urata, J. Vac. Sci. Technol. A **23**, 938 (2005).
[35]D. Chin, S. H. Dhong, and G. J. Long, J. Electrochem. Soc. **132**, 1705 (1985).
[36]O. Joubert, G. S. Oehrlein, and M. Surendra, J. Vac. Sci. Technol. A **12**, 665 (1994).
[37]M. F. Doemling, N. R. Rueger, and G. S. Oehrlein, Appl. Phys. Lett. **68**, 10 (1996).
[38]R. Knizikevicius, Vacuum **72**, 53 (2003).
[39]J.-N. Sun, D. W. Gidley, Y. Hu, W. E. Frieze, and E. T. Ryan, Appl. Phys. Lett. **81**, 1447 (2002).
[40]N. Posseme, T. Chevolleau, T. David, M. Darnon, O. Louveau, and O. Joubert, J. Vac. Sci. Technol. B **25**, 1928 (2007).
[41]N. Rochat, A. Chabli, F. Bertin, M. Olivier, C. Vergnaud, and P. Mur, J. Appl. Phys. **91**, 5029 (2002).
[42]S. G. Ingram, J. Appl. Phys. **68**, 500 (1990).
[43]S. A. Vitale and H. H. Sawin, J. Vac. Sci. Technol. A **20**, 651 (2002).
[44]T. Kwon, H.-C. Kan, G. S. Oehrlein, and R. J. Phaneuf, Nanotechnology **18**, 055305 (2007).
[45]M. Darnon, T. Chevolleau, D. Eon, R. Bouyssou, B. Pelissier, L. Vallier, O. Joubert, N. Posseme, T. David, F. Bailly, and J. Torres, Microelectron. Eng. **85**, 2226 (2008).
[46]S. Demuynck, H. Kim, C. Huffman, M. Darnon, H. Struyf, J. Versluijs, M. Claes, G. Vereecke, P. Verdonck, H. Volders, N. Heylen, K. Kellens, D. De Roest, H. Sprey, and G. Beyer, Jpn. J. Appl. Phys. **48**, 04C018 (2009).
[47]O. Hinsinger, R. Fox, E. Sabouret, C. Goldberg, C. Verove, W. Besling, P. Brun, E. Josse, C. Monjet, O. Belmont, J. Van Hassel, B. G. Sharma, J. P. Jacquemin, P. Vannier, A. Humbert, D. Bunel, R. Gonella, E. Mastromatteo, D. Reber, A. Farcy, J. Mueller, P. Christie, V. H. Nguyen, C. Cregut, and T. Berger, Tech. Dig. - Int. Electron Devices Meet. **2004**, 317.
[48]J.-F. de Marneffe, D. Goossens, D. Hendrickx, H. Struyf, T. Conard, A. Franquet, and W. Boullart, Plasma Etch and Strip in Microelectronics Conference, 2nd ed., Leuven, 2009, (http://www.pesm2009.be).
[49]N. Posseme, T. David, M. Darnon, T. Chevolleau, and O. Joubert, *6th International Conference on Microelectronics and Interfaces*, 2005 (unpublished).